

A One-Dimensional Symmetric Force-Based Blending Method for Atomistic-to-Continuum Coupling

Elaine Gorom-Alexander*

Xingjie Helen Li[†]

April 28, 2023

Abstract

Inspired by the blending method developed by [P. Seleson, S. Beneddine, and S. Prudhome, *A Force-Based Coupling Scheme for Peridynamics and Classical Elasticity*, (2013)] for the nonlocal-to-local coupling, we create a symmetric and consistent blended force-based Atomistic-to-Continuum (a/c) scheme for the atomistic chain in one-dimensional space. The conditions for the well-posedness of the underlying model are established by analyzing an optimal blending size and blending type to ensure the H^1 semi-norm stability for the blended force-based operator. We present several numerical experiments to test and confirm the theoretical findings.

Keywords: atomistic-to-continuum coupling, symmetric force-based blending, stability and blending size analysis

1 Introduction

Many important materials from airplane wings to computer chips can be improved by a better understanding of failure modes such as fracture and fatigue. Thus, one of the most important goals of computational materials science is to efficiently and reliably predict phenomena such as crack growth and to facilitate the design of new materials better able to resist failure. Scientists and engineers have proposed several multi-scale methods (e.g., [12, 17, 6, 7, 4, 8, 16, 13, 14, 19]) to overcome the computational challenges in fidelity and efficiency.

The two main strategies in multi-scale modelings are: (1) bottom-up atomistic-to-continuum: coarse-graining of microscopic descriptions (e.g., atomistic models) of material behavior [11, 17, 6, 15, 10]; (2) top-down local-to-nonlocal: informing macroscopic models (e.g., continuum equations) with physics gleaned from the microscopic scales [16, 4, 13, 14, 5, 1, 3, 19, 2, 18, 20]. The former provides a "closer" comparison with macroscopic experiments, and the latter predicts the materials' microscopic properties [8]. Meanwhile, the two approaches have many interconnections, and their development and understanding often inspire each other.

In this work, we employ a symmetric blending strategy developed by P Seleson *et. al.* for the nonlocal-to-local coupling [13, 14] and develop a new force-based atomistic-to-continuum model for a 1D atomistic chain. We then study the stability property of the new coupling scheme in terms of the blending function and its blending size using similar mathematical tools from [9]. We investigate the optimal number of atoms within the blending region to ensure the positive-definiteness of the resulting force blending operator under the discrete H^1 semi-norm. The results admit a very narrow blending region to maintain the coercivity and efficiency when the number of atoms is large. In addition, the stability analysis developed in this work is crucial for the convergence for several popular iterative methods for solving large-force equilibrium systems.

We will arrange the paper as follows. In section 2, we introduce the force-based symmetric blending method for a 1D atomistic chain. We construct an atomistic, linearized force equation and a continuum,

*Department of Mathematics and Statistics, University of North Carolina at Charlotte, Email: egorom@uncc.edu

[†]Department of Mathematics and Statistics, University of North Carolina at Charlotte, Email: xli47@uncc.edu

linearized force equation from the atomistic energy equation. The consistency between these methods is discussed in Proposition 2.2. A blending function is then introduced to symmetrically combine these two force-based equations.

In section 3, we establish the optimal conditions on the size of the blending region for the blending force operator with respect to the H^1 stability. Theorem 3.1 and Theorem 3.2 establish these conditions.

In section 4, a uniform stretch is applied to compute the critical strain errors for various types of blending functions with different blending sizes. It is found that the cubic blending function is optimal.

We find that a larger polynomial size on the blending region is suggested from the numerical trials when the number of atoms in the chain is just moderately large.

Also in section 4, we test a sine and Gaussian external force to the system to model the displacement with our force-based blending method. The displacements produced by the blending methods with sufficient blending size agree with those of fully atomistic models. In addition, we compare the impact of interaction range of the atomistic model, and observe that an interaction range potential greater than 2 neighbors does not change the displacement significantly.

2 Derivation of the Symmetric and Consistent Force-Based Scheme

In this section, we will introduce notations, introduce the reference atomistic model, and then derive the continuum approximation. After this, we introduce a blending equation to symmetrically combine these two models. Utilizing this blending equation, a coupling scheme for the blended atomistic and continuum forces is created.

2.1 Notations

We consider a 1D atomistic chain with finite interaction range up to the N -th nearest neighbor and a total number of $2M$ atoms within the domain Ω . We denote the scaled reference lattice $x_\ell = a\ell$ for $\ell \in \mathbb{Z}$ with fixed reference lattice spacing constant $a := \frac{1}{M}$ such that we can select a reference domain which is fixed to be $\Omega = (-1, 1]$. Throughout, the interaction range N will be fixed. The chain is deformed to a current configuration $y_\ell = x_\ell + u_\ell$.

The displacement field $u = (u_\ell)_{\ell \in \mathbb{Z}} : \mathbb{Z} \rightarrow \mathbb{R}$ is assumed to be $2M$ periodic discrete function and \mathcal{U} denotes the space of all $2M$ periodic displacement functions

$$\mathcal{U} := \{u : u_{\ell+2M} = u_\ell | \ell \in \mathbb{Z}\}.$$

Accordingly, we set the deformation space by

$$\mathcal{Y} := \{y : y_\ell = x_\ell + u_\ell | u \in \mathcal{U}, \ell \in \mathbb{Z}\}.$$

We also define the discrete differentiation operator for simplicity, u' , on periodic displacements by

$$u'_\ell := \frac{u_{\ell+1} - u_\ell}{a}.$$

Then we may define the higher-order discrete differentiation u'' , $u^{(3)}$, and $u^{(4)}$ for ℓ by

$$\begin{cases} u''_\ell := \frac{u'_\ell - u'_{\ell-1}}{a}, \\ u^{(3)}_\ell := \frac{u''_{\ell+1} - u''_\ell}{a}, \\ u^{(4)}_\ell := \frac{u^{(3)}_\ell - u^{(3)}_{\ell-1}}{a}. \end{cases} \quad (2.1)$$

For a displacement $u \in \mathcal{U}$ and its discrete derivatives, we employ the discrete ℓ^2 and ℓ^∞ norms by

$$\|u\|_{\ell^2}^2 := \sum_{\ell=-M+1}^M |u_\ell|^2 a, \quad \text{and} \quad \|u\|_{\ell^\infty} := \max_{-M+1 \leq \ell \leq M} |u_\ell|. \quad (2.2)$$

In particular, the associated inner product for ℓ_2 is

$$\langle u, w \rangle := \sum_{\ell=-M+1}^M u_\ell w_\ell a.$$

We also employ the discrete H^1 semi norm, $|u|_{H^1}^2 = \|u'\|_{\ell_2}^2$ in the stability analysis.

Meanwhile, we proceed with $\tilde{u} : \mathbb{R} \rightarrow \mathbb{R}$ as a quintic spline interpolation of u such that

$$\begin{aligned} \tilde{u}(a\ell) &= u_\ell, \\ \tilde{u}(-Ma) &= \tilde{u}(Ma), \\ \lim_{t \rightarrow (a\ell)^-} \frac{d^\omega \tilde{u}}{dx^\omega}(t) &= \lim_{t \rightarrow (a\ell)^+} \frac{d^\omega \tilde{u}}{dx^\omega}(t), \quad \omega = 1, \dots, 4 \end{aligned} \tag{2.3}$$

As \tilde{u} is a continuous function, we can introduce notations for its derivatives, for instance, \tilde{u}_x as its first derivative at $(a\ell)$, and \tilde{u}_{xx} as its second derivative at $(a\ell)$, etc.

We can compare the derivatives of $\tilde{u}(x)$ with the differencing of u_ℓ . Clearly, we have

$$\begin{aligned} u'_\ell &= \tilde{u}_x(a\ell) + \frac{a}{2} \tilde{u}_{xx}(\tilde{\xi}) \\ u''_\ell &= \tilde{u}_{xx}(a\ell) + \frac{a^2}{12} \tilde{u}_{xxx}(\tilde{\xi}) \end{aligned} \tag{2.4}$$

Note that throughout, subscript ℓ is used to denote when discrete differentiation is employed; whereas subscript x is used to denote when considering the true derivatives.

As in [9], we will frequently use the following discrete summation by parts identity:

Lemma 2.1. *Suppose $\{u_\ell\}_{\ell=a+1}^b$ and $\{v_\ell\}_{\ell=a+1}^b$ are two sequences, then we have*

$$\sum_{\ell=a+1}^b u_\ell (v_\ell - v_{\ell-1}) = [u_b v_b - u_a v_a] - \sum_{\ell=a+1}^b (u_\ell - u_{\ell-1}) v_{\ell-1}.$$

Furthermore, when both $\{u_\ell\}_{\ell=a+1}^b$ and $\{v_\ell\}_{\ell=a+1}^b$ are periodic sequences with $u(a) = u(b)$ and $v(a) = v(b)$, we have

$$\sum_{\ell=a+1}^b u_\ell (v_\ell - v_{\ell-1}) = - \sum_{\ell=a+1}^b (u_\ell - u_{\ell-1}) v_{\ell-1}.$$

We use this lemma to find conditions on coupling to ensure the positive-definiteness of the bilinear form of the symmetric, blended force-based operator.

2.2 1D atomistic and continuum models

Energy formulations and consistency analysis.

We now consider a one-dimensional atomistic periodic chain deformed into configuration $y \in \mathcal{Y}$. Recall that the atomistic periodicity is fixed to $2M$, and the interaction range is fixed to N -th neighbors. The total atomistic energy for this periodic chain is given by

$$E^{a,tot}(y) := \sum_{\ell=-M+1}^M \sum_{\substack{k=-N, \\ k \neq 0}}^N \frac{a}{2} \phi\left(\frac{y_{\ell+k} - y_\ell}{a}\right), \tag{2.5}$$

where $\phi(\cdot) : \mathbb{R} \rightarrow \mathbb{R}$ is a Lennard-Jones type potential. It can also be viewed as the energy density per unit volume for pairwise interactions. We assume that $\phi(\cdot)$ has the following properties:

- $\phi(r) = \phi(|r|)$;

- ϕ is at least four times differentiable; and
- $\phi_{xx}(1) > 0$ and $\phi_{xx}(k) \leq 0$ for $k \geq 2$.

In the numerical simulation, we employ the Morse potential, and a graphical illustration can be found in Figure 1.

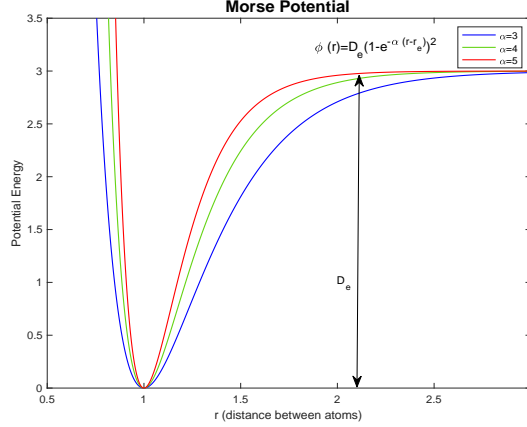


Figure 1: Graphical illustration of the Lennard-Jones type interaction potential (Morse potential) used in numerical experiments. Notice that the local minimum is achieved at the nearest neighbour distance $r = r_e$.

Next, we derive the continuum model by only using the first neighbor distance, that is we only use the differencing u'_ℓ as we approximate the argument for ϕ . For $k = 2, \dots, N$, we have

$$\begin{aligned} \frac{y_{\ell+k} - y_\ell}{a} &= \frac{x_{\ell+k} - x_\ell + u_{\ell+k} - u_\ell}{a} \\ &= k + u'_\ell + \sum_{j=1}^{k-1} u'_{\ell+j}, \end{aligned}$$

Using the error estimates listed in (2.4), we can replace $u'_{\ell+j}$ by u'_ℓ and estimate the discrepancy

$$\begin{aligned} \frac{y_{\ell+k} - y_\ell}{a} &= k + u'_\ell + \sum_{j=1}^{k-1} \tilde{u}_x(a(\ell+j)) + c_1 a \\ &= k + u'_\ell + \sum_{j=1}^{k-1} \tilde{u}_x((a\ell)) + c_2 a \\ &= k + ku'_\ell + c_3 a, \end{aligned} \tag{2.6}$$

where c_1, c_2 and c_3 are constants depending on k and regularity of \tilde{u} . For $k = -N, \dots, -2$, we can obtain similar consistency estimates.

The atomistic energy equation is rooted in discrete, nonlocal energy descriptions. Assuming the finest mesh with each atom regarded as a node and substituting the previous approximation into the atomistic energy (2.5), we thus defined the continuum energy as

$$E^c(u) := \sum_{\ell=-M+1}^M \sum_{\substack{k=-N \\ k \neq 0}}^N \frac{a}{2} \phi(k + ku'_\ell). \tag{2.7}$$

So far, both the atomistic energy and the continuum energy are non-linearly dependent on the displacement field $\{u_\ell\}_{\ell=-M+1}^M$, and we would like to apply further simplifications to obtain linear models. To linearize

the total atomistic energy, we follow a similar argument as deriving the continuum energy,

$$\begin{aligned}\frac{y_{\ell+k} - y_\ell}{a} &= \frac{x_{\ell+k} - x_\ell + u_{\ell+k} - u_\ell}{a} \\ &= k + \frac{u_{\ell+k} - u_\ell}{a}.\end{aligned}$$

Therefore, the total atomistic energy can be written as

$$\begin{aligned}E^{a,tot}(y) &:= \sum_{\ell=-M+1}^M \sum_{\substack{k=-N, \\ k \neq 0}}^N \frac{a}{2} \phi\left(\frac{y_{\ell+k} - y_\ell}{a}\right) \\ &= \sum_{\ell=-M+1}^M \sum_{\substack{k=-N, \\ k \neq 0}}^N \frac{a}{2} \phi\left(k + \frac{u_{\ell+k} - u_\ell}{a}\right)\end{aligned}\tag{2.8}$$

Next, we utilize Taylor expansion to $\phi\left(k + \frac{u_{\ell+k} - u_\ell}{a}\right)$ at the reference configuration to linearize the expression.

$$\phi\left(k + \frac{u_{\ell+k} - u_\ell}{a}\right) = \phi(k) + \frac{u_{\ell+k} - u_\ell}{a} \phi_x(k) + \frac{1}{2} \left(\frac{u_{\ell+k} - u_\ell}{a}\right)^2 \phi_{xx}(k) + O\left(\left(\frac{u_{\ell+k} - u_\ell}{a}\right)^3\right).$$

Inserting the Taylor approximation into the atomistic energy equation (2.8), we obtain

$$\sum_{\ell=-M+1}^M \sum_{\substack{k=-N, \\ k \neq 0}}^N \frac{a}{2} \left[\phi(k) + \frac{u_{\ell+k} - u_\ell}{a} \phi_x(k) + \frac{1}{2} \left(\frac{u_{\ell+k} - u_\ell}{a}\right)^2 \phi_{xx}(k) + O\left(\left(\frac{u_{\ell+k} - u_\ell}{a}\right)^3\right) \right].\tag{2.9}$$

Then, without loss of generality, we assume $\sum_{\substack{k=-N, \\ k \neq 0}}^N \phi(k) = 0$ since this term will not contribute to force. Also, since the reference configuration is a local minimizer and the potential is symmetric, we have

$$\sum_{\substack{k=-N, \\ k \neq 0}}^N \frac{u_{\ell+k} - u_\ell}{a} \phi_x(k) = 0.$$

Thus, the linearized atomistic energy is

$$E^{a,lin}(u) := \sum_{\ell=-M+1}^M \sum_{\substack{k=-N, \\ k \neq 0}}^N \frac{a}{2} \left(\frac{1}{2} \left(\frac{u_{\ell+k} - u_\ell}{a}\right)^2 \phi_{xx}(k) \right).\tag{2.10}$$

Following the linearization of the atomistic energy, for the continuum energy, we utilize Taylor expansion to $\phi(k + ku'_\ell)$ at the reference configuration to linearize the expression

$$\phi(k + ku'_\ell) = \phi(k) + ku'_\ell \phi_x(k) + \frac{1}{2} (ku'_\ell)^2 \phi_{xx}(k) + O\left((ku'_\ell)^3\right).$$

Inserting the Taylor approximation into the continuum energy equation (2.7), we obtain

$$\sum_{\ell=-M+1}^M \sum_{\substack{k=-N, \\ k \neq 0}}^N \frac{a}{2} \left(\phi(k) + ku'_\ell \phi_x(k) + \frac{1}{2} (ku'_\ell)^2 \phi_{xx}(k) + O\left((ku'_\ell)^3\right) \right).\tag{2.11}$$

Following the same justification as above regarding the terms of the Taylor expansion, the linearized continuum energy associated with the finest mesh is defined as

$$\begin{aligned} E^{c,lin}(u) &:= \sum_{\ell=-M+1}^M \sum_{\substack{k=-N, \\ k \neq 0}}^N \frac{a}{2} \left(\frac{k^2}{2} (u'_\ell)^2 \phi_{xx}(k) \right) \\ &= \sum_{\ell=-M+1}^M \left(\sum_{k=1}^N \frac{k^2}{2} \phi_{xx}(k) \right) (u'_\ell)^2 a. \end{aligned} \quad (2.12)$$

Remark 2.1. Notice that the classical continuum mechanics for interaction range up to the N -th nearest neighbour has the following form:

$$\tilde{E}^{c,lin}(\tilde{u}) = \int W \left(\frac{d\tilde{u}}{dx} \right)^2 dx \quad (2.13)$$

where $\frac{d\tilde{u}}{dx}$ is the deformation field and W represents the strain energy density

$$W := \sum_{k=1}^N \frac{k^2}{2} \phi_{xx}(k). \quad (2.14)$$

Notice that if we use a fine mesh and applying a Riemann sum to approximate the integral of (2.13), we can convert (2.13) into (2.12). Therefore, the linearized continuum energy for a discrete lattice system is consistent with the theory of classical continuum mechanics. For the consistency between the classical continuum mechanics and the linearized continuum energy, we refer to Section 7 as it follows closely with the consistency for the linearized continuum energy equation and the atomistic energy description.

Since we obtain the atomistic and continuum energies, in the next proposition, we will summarize the truncation errors.

Proposition 2.1 (Consistency Analysis of Linearized Energy Formulations). *Given a fully refined continuum mesh on the 1D atomistic chain, we derive the linearized continuum energy equation (2.12),*

$$E^{c,lin}(u) := \sum_{\ell=-M+1}^M \sum_{\substack{k=-N, \\ k \neq 0}}^N \frac{a}{2} \left(\frac{k^2}{2} (u'_\ell)^2 \phi_{xx}(k) \right).$$

from the atomistic energy description, (2.5),

$$E^{a,lin}(u) := \sum_{\ell=-M+1}^M \sum_{\substack{k=-N, \\ k \neq 0}}^N \frac{a}{2} \left(\frac{1}{2} \left(\frac{u_{\ell+k} - u_\ell}{a} \right)^2 \phi_{xx}(k) \right).$$

with the deformed configuration and the displacement field linked by $y_\ell = x_\ell + u_\ell$. Then, the consistency between the linearized continuum energy equation and the atomistic energy equation is $O(a^2)$.

Proof. Comparing $E^{c,lin}$ and $E^{a,lin}$, we have

$$E^{c,lin} - E^{a,lin} = \sum_{\ell=-M+1}^M \sum_{\substack{k=-N, \\ k \neq 0}}^N \frac{a}{2} \left(\frac{k^2}{2} (u'_\ell)^2 \phi_{xx}(k) \right) - \sum_{\ell=-M+1}^M \sum_{\substack{k=-N, \\ k \neq 0}}^N \frac{a}{2} \left(\frac{1}{2} \left(\frac{u_{\ell+k} - u_\ell}{a} \right)^2 \phi_{xx}(k) \right).$$

For any $k = 2, \dots, N$, we compare $u_{\ell+k}$ around ℓ . Recall the quintic spline interpolation \tilde{u} defined in (2.3), we have

$$u_{\ell+k} = u_\ell + ka\tilde{u}_x + O(a^2).$$

Thus, for all k ,

$$u_{\ell+k} - u_\ell = ka\tilde{u}_x + O(a^2).$$

Then, the consistency analysis of energies yields:

$$\begin{aligned}
& E^{c,lin} - E^{a,lin} \\
&= \sum_{\ell=-M+1}^M \sum_{\substack{k=-N, \\ k \neq 0}}^N \frac{a}{2} \left(\frac{k^2}{2} (u'_\ell)^2 \phi_{xx}(k) \right) - \sum_{\ell=-M+1}^M \sum_{\substack{k=-N, \\ k \neq 0}}^N \frac{a}{2} \left(\frac{1}{2} \left(\frac{u_{\ell+k} - u_\ell}{a} \right)^2 \phi_{xx}(k) \right) \\
&= \sum_{\ell=-M+1}^M \sum_{\substack{k=-N, \\ k \neq 0}}^N \frac{a}{2} \left(\frac{k^2}{2} \left(\frac{u_{\ell+1} - u_\ell}{a} \right)^2 \phi_{xx}(k) \right) - \sum_{\ell=-M+1}^M \sum_{\substack{k=-N, \\ k \neq 0}}^N \frac{a}{2} \left(\frac{1}{2} \left(\frac{u_{\ell+k} - u_\ell}{a} \right)^2 \phi_{xx}(k) \right) \\
&= \sum_{\ell=-M+1}^M \sum_{\substack{k=-N, \\ k \neq 0}}^N \frac{a}{2} \left(\frac{k^2}{2} \left(\frac{a\tilde{u}_x + O(a^2)}{a} \right)^2 \phi_{xx}(k) \right) - \sum_{\ell=-M+1}^M \sum_{\substack{k=-N, \\ k \neq 0}}^N \frac{a}{2} \left(\frac{1}{2} \left(\frac{ka\tilde{u}_x + O(a^2)}{a} \right)^2 \phi_{xx}(k) \right) \\
&= \sum_{\ell=-M+1}^M \sum_{\substack{k=-N, \\ k \neq 0}}^N \frac{a}{2} \frac{k^2}{2} \phi_{xx}(k) + O(a^2) - \sum_{\ell=-M+1}^M \sum_{\substack{k=-N, \\ k \neq 0}}^N \frac{a}{2} \frac{k^2}{2} \phi_{xx}(k) + O(a^2) \\
&= O(a^2).
\end{aligned}$$

□

Next, we derive the formulae of forces for both linear atomistic and continuum models. Because the mesh is fully refined, the linearized continuum force of atom ℓ can be obtained from taking the first order variation of the linearized continuum energy (2.12) with respect to u_ℓ , we thus get:

$$\begin{aligned}
F_{\ell}^{c,lin}(u) &:= \frac{1}{a} \frac{\delta E^{c,lin}(u)}{\delta u_\ell} = \frac{\delta \left[\sum_{j=-M+1}^M \left(\sum_{k=1}^N \frac{k^2}{2} \phi_{xx}(k) \right) (u_j')^2 \right]}{\delta u_\ell} \\
&= - \left(\left(\sum_{k=1}^N \frac{k^2}{2} \phi_{xx}(k) \right) \frac{2(u_{\ell+1} - u_\ell)}{a^2} - \left(\sum_{k=1}^N \frac{k^2}{2} \phi_{xx}(k) \right) \frac{2(u_\ell - u_{\ell-1})}{a^2} \right) \\
&= - \left(\sum_{k=1}^N k^2 \phi_{xx}(k) \right) u_\ell'',
\end{aligned} \tag{2.15}$$

where we recall the shorthand notation u_ℓ'' as

$$u_\ell'' := \frac{u_{\ell+1} - 2u_\ell + u_{\ell-1}}{a^2}.$$

For the atomistic forces, we recall $y_\ell = x_\ell + u_\ell$, take the first order variation of the total atomistic energy (2.5) at atom ℓ and notice we employ the forward finite-differencing, hence, we obtain

$$\begin{aligned}
F_{\ell}^a(u) &:= \frac{\delta E^{a,tot}}{\delta u_\ell} = \frac{\delta}{\delta u_\ell} \sum_{j=-M+1}^M \sum_{\substack{k=-N, \\ k \neq 0}}^N \frac{1}{2} \phi \left(\frac{y_{j+k} - y_j}{a} \right) \\
&= - \sum_{\substack{k=-N, \\ k \neq 0}}^N \frac{1}{2a} \left(\phi_x \left(k + \frac{u_{\ell+k} - u_\ell}{a} \right) - \phi_x \left(k + \frac{u_\ell - u_{\ell-k}}{a} \right) \right).
\end{aligned} \tag{2.16}$$

Linearizing the forces around the reference configuration by applying Taylor expansion to $\phi_x(\cdot)$, we obtain the linearized atomistic forces

$$F_{\ell}^{a,lin}(u) := - \sum_{\substack{k=-N, \\ k \neq 0}}^N \frac{1}{2} \phi_{xx}(k) \left(\frac{u_{\ell+k} - 2u_\ell + u_{\ell-k}}{a^2} \right) = - \sum_{k=1}^N \phi_{xx}(k) \left(\frac{u_{\ell+k} - 2u_\ell + u_{\ell-k}}{a^2} \right). \tag{2.17}$$

In the next proposition, we summarize the consistency errors between the linearized atomistic and linearized continuum forces.

Proposition 2.2 (Consistency analysis of force). *Given a fully refined continuum mesh on the 1D atomistic chain, the linearized atomistic force equation (2.17) for atom ℓ is*

$$F_{\ell}^{a,lin}(u) := - \sum_{k=1}^N \phi_{xx}(k) \left(\frac{u_{\ell+k} - 2u_{\ell} + u_{\ell-k}}{a^2} \right)$$

and the linearized continuum force equation (2.15) for node ℓ is

$$F_{\ell}^{c,lin}(u) = - \left(\sum_{k=1}^N k^2 \phi_{xx}(k) \right) u_{\ell}''.$$

Thus, the consistency error between (2.17) and (2.15) is $O(a^2)$.

Proof. Comparing $F_{\ell}^{c,lin}$ and $F_{\ell}^{a,lin}$, we have

$$F_{\ell}^{c,lin}(u) - F_{\ell}^{a,lin}(u) = - \sum_{k=1}^N \phi_{xx}(k) \left(k^2 u_{\ell}'' \right) + \sum_{k=1}^N \phi_{xx}(k) \left(\frac{u_{\ell+k} - 2u_{\ell} + u_{\ell-k}}{a^2} \right).$$

For any $k = 2, \dots, N$, we compare $u_{\ell+k}$ and $u_{\ell-k}$ around ℓ . Recall the quintic spline interpolation \tilde{u} defined in (2.3), we have

$$\begin{aligned} u_{\ell+k} &= \tilde{u}(a(\ell+k)) - \tilde{u}(a\ell) + \tilde{u}(a\ell) = u_{\ell} + ka\tilde{u}_x + \frac{1}{2}(ka)^2\tilde{u}_{xx} + \frac{1}{6}(ka)^3\tilde{u}_{xxx} + O(a^4), \\ u_{\ell-k} &= \tilde{u}(a(\ell-k)) - \tilde{u}(a\ell) + \tilde{u}(a\ell) = u_{\ell} - ka\tilde{u}_x + \frac{1}{2}(ka)^2\tilde{u}_{xx} - \frac{1}{6}(ka)^3\tilde{u}_{xxx} + O(a^4). \end{aligned}$$

Utilizing this Taylor expansion for the atomistic and continuous linear force equations, the consistency analysis yields

$$\begin{aligned} F_{\ell}^{c,lin}(u) - F_{\ell}^{a,lin}(u) &= - \sum_{k=1}^N \phi_{xx}(k) \left(k^2 u_{\ell}'' \right) + \sum_{k=1}^N \phi_{xx}(k) \left(\frac{u_{\ell+k} - 2u_{\ell} + u_{\ell-k}}{a^2} \right) \\ &= - \sum_{k=1}^N \phi_{xx}(k) \left(k^2 \frac{u_{\ell+1} - 2u_{\ell} + u_{\ell-1}}{a^2} \right) + \sum_{k=1}^N \phi_{xx}(k) \left(k^2 \tilde{u}_{xx} + O(a^2) \right) \\ &= - \sum_{k=1}^N \phi_{xx}(k) \left(k^2 \tilde{u}_{xx} + O(a^2) \right) + \sum_{k=1}^N \phi_{xx}(k) \left(k^2 \tilde{u}_{xx} + O(a^2) \right) \\ &= O(a^2). \end{aligned}$$

A more thorough proof can be seen in Subsection 7.1. □

Remark 2.2. Notice that a is chosen to be $\frac{1}{M}$ with M being large, hence, the consistency error becomes small when the number of atoms within Ω is sufficiently large.

2.3 Derivation of a Symmetric Blending Model for the AtC Coupling

In this section we will derive a symmetric and consistent force-based atomistic-to-continuum scheme for the 1D atomistic chain.

We first divide the domain of interest into three distinct sub-domains: Ω^a : the domain described by the atomistic force; Ω^c : the domain described by the continuum force; and Ω^b : the blending region where the atomistic and continuum force models are both used.

We now introduce a smooth blending function β that can be defined as such:

Definition 2.1 (Definition of blending function). We may define a smooth blending function β_ℓ such that:

$$\beta_\ell = \begin{cases} 1, & \ell \in \Omega^a \\ 0, & \ell \in \Omega^c \\ \in (0, 1), & \ell \in \Omega^b. \end{cases} \quad (2.18)$$

This blending function can take many forms and we will employ linear spline, cubic spline, and quintic spline blending functions in the numerical experiments in Section 4.

Notice that creating a linearized force equation will give way to easier analysis in studying the stability of the scheme and providing insights on the coupling conditions of more general cases, so we focus on blending the linearized atomistic and continuum forces. In order for consistent symmetry, we start from $k = -N, \dots, N$, and $k \neq 0$. Consequently, we start from the linearized, atomistic force equation in (2.17) and incorporate the blending function β_ℓ as follows:

$$\begin{aligned} F_{\ell,}^{a,lin} &:= - \sum_{k=1}^N \phi_{xx}(k) \frac{u_{\ell+k} - 2u_\ell + u_{\ell-k}}{a^2} = - \sum_{\substack{k=-N, \\ k \neq 0}}^N \frac{1}{2} \phi_{xx}(k) \frac{u_{\ell+k} - 2u_\ell + u_{\ell-k}}{a^2} \\ &= - \sum_{\substack{k=-N, \\ k \neq 0}}^N \left(\frac{\beta_\ell + \beta_{\ell+k}}{2} \right) \frac{1}{2} \phi_{xx}(k) \frac{u_{\ell+k} - 2u_\ell + u_{\ell-k}}{a^2} - \sum_{\substack{k=-N, \\ k \neq 0}}^N \left(1 - \frac{\beta_\ell + \beta_{\ell+k}}{2} \right) \frac{1}{2} \phi_{xx}(k) \frac{u_{\ell+k} - 2u_\ell + u_{\ell-k}}{a^2}, \end{aligned}$$

such that the term $\frac{u_{\ell+|k|} - 2u_\ell + u_{\ell-|k|}}{a^2}$ is multiplied by the pair $\left(\frac{\beta_\ell + \beta_{\ell+|k|}}{2} \right)$ and $\left(\frac{\beta_\ell + \beta_{\ell-|k|}}{2} \right)$, respectively. Next, we further simplify and get

$$\begin{aligned} F_{\ell,}^{a,lin} &= - \sum_{k=1}^N \left(\frac{\beta_{\ell-k} + 2\beta_\ell + \beta_{\ell+k}}{4} \right) \phi_{xx}(k) \frac{u_{\ell+k} - 2u_\ell + u_{\ell-k}}{a^2} \\ &\quad - \sum_{k=1}^N \left(1 - \frac{\beta_{\ell-k} + 2\beta_\ell + \beta_{\ell+k}}{4} \right) \phi_{xx}(k) \frac{u_{\ell+k} - 2u_\ell + u_{\ell-k}}{a^2}. \end{aligned} \quad (2.19)$$

Then, we approximate the second term of the equation by using the linearized continuum portion. Therefore, we get the blended force function which is defined as:

$$\begin{aligned} F_{\ell,}^{bqcf,lin}(u) &:= - \sum_{k=1}^N \left(\frac{\beta_{\ell-k} + 2\beta_\ell + \beta_{\ell+k}}{4} \right) \phi_{xx}(k) \frac{u_{\ell+k} - 2u_\ell + u_{\ell-k}}{a^2} \\ &\quad - \sum_{k=1}^N \left(1 - \frac{\beta_{\ell-k} + 2\beta_\ell + \beta_{\ell+k}}{4} \right) \phi_{xx}(k) k^2 \frac{u_{\ell+1} - 2u_\ell + u_{\ell-1}}{a^2} \\ &= - \sum_{k=1}^N \left(\frac{\beta_{\ell-k} + 2\beta_\ell + \beta_{\ell+k}}{4} \right) \phi_{xx}(k) \frac{u_{\ell+k} - 2u_\ell + u_{\ell-k}}{a^2} - \sum_{k=1}^N \left(1 - \frac{\beta_{\ell-k} + 2\beta_\ell + \beta_{\ell+k}}{4} \right) \phi_{xx}(k) k^2 u_\ell''. \end{aligned} \quad (2.20)$$

Remark 2.3. As $\ell - k$ and $\ell + k$ are both employed in the term of the blending function, this blending operator is symmetric as in [13].

We also see that the first term recovers (2.17) for $\beta \equiv 0$, and the second term recovers (2.15) for $\beta \equiv 1$. Thus, the consistency error between the linearized $F_{\ell,}^{bqcf,lin}$ and $F_{\ell,}^{a,lin}$ is also of $O(a^2)$.

3 Stability Analysis for the Linearized Blending Model

3.1 Bilinear Form of Linearized Blending Model

In this section we study the size of the blending region with respect to the H^1 stability of the blending operator. This is achieved by obtaining the optimal conditions in which the linearized coupling operator is positive definite under the discrete H^1 semi-norm.

From (2.20), we consider the bilinear form

$$\langle F_{,1}^{bqcf,lin}(u), v \rangle = \langle F_{,1}^{bqcf,lin}(u), v \rangle + \sum_{k=2}^N \langle F_k^{bqcf,lin}(u), v \rangle, \quad \forall v \in \mathcal{U}, \quad (3.1)$$

where the first neighbor interaction—the first term—is set apart due to its simplicity in analysis. The second term accounts for the next-nearest neighbor to the N -th nearest neighbor.

To observe the stability of the operator, we first look at the nearest and next-nearest neighbor interaction, for simplicity as well as for the coercivity assumption on $\phi_{xx}(1) > 0$ and $\phi_{xx}(k) \leq 0$ with $k \geq 2$, to find the constraints on the size of blending region. Then, we discuss how the next-nearest neighbor analysis can be extended to the general N -th neighbor interaction.

The discrete stability analysis is inspired by and similar to the analogous continuous analysis for the force-based operator that can be seen in the Appendix 7. We proceed with the analysis for the discrete case.

3.2 Stability Analysis for Next-Nearest Neighbor Interaction Range: $N = 2$.

Lemma 3.1. *For any displacements $u = (u_\ell)_{\ell=-M+1}^M$ from the deformed configuration $y_\ell = x_\ell + u_\ell$, the bilinear forms of nearest neighbor and the next-nearest neighbor interaction operator can be written as*

$$\begin{aligned} \langle F_{,1}^{bqcf,lin}(u), u \rangle &= \phi_{xx}(1) \left\| u' \right\|_{\ell_2}^2 \\ \langle F_{,2}^{bqcf,lin}(u), u \rangle &= 2 \left\{ 2\phi_{xx}(2) \left\| u' \right\|_{\ell_2}^2 - \frac{\phi_{xx}(2)}{2} a^2 \left\| \sqrt{\beta} u'' \right\|_{\ell_2}^2 + \frac{\phi_{xx}(2)}{2} a^2 \left\| \sqrt{|\beta''|} |u'| \right\|_{\ell_2}^2 + R + S \right\}. \end{aligned} \quad (3.2)$$

where

$$R := \sum_{\ell=-M+1}^M \frac{\phi_{xx}(2)}{2} \left(u'_\ell \beta_{\ell-1}^{(3)}(u_{\ell-1}) - u''_\ell \beta''_\ell u'_\ell a \right) a^3$$

and

$$S := \sum_{\ell=-M+1}^M \frac{\phi_{xx}(2)}{2} (u'_\ell a)^2 \left(\beta'_\ell u'_\ell - \beta'_{\ell-2} u'_{\ell-2} \right).$$

Proof. For the nearest neighbor interaction, as the $F^{a,lin}$ and $F^{c,lin}$ coincide, we have

$$\begin{aligned} \langle F_{,1}^{bqcf,lin}(u), u \rangle &= - \sum_{\ell=-M+1}^M \left[\phi_{xx}(1) a \left(\frac{u_{\ell+1} - 2u_\ell + u_{\ell-1}}{a^2} \right) \right] u_\ell \\ &= - \sum_{\ell=-M+1}^M \phi_{xx}(1) u''_\ell u_\ell a. \end{aligned}$$

Then, using the discrete derivative and summation by parts formula from Lemma 2.1, we conclude that

$$\langle F_{,1}^{bqcf,lin}(u), u \rangle = - \sum_{\ell=-M+1}^M \phi_{xx}(1) u''_\ell u_\ell a = \phi_{xx}(1) \left\| u' \right\|_{\ell_2}^2.$$

For, the next-nearest neighbor interaction, recall from (2.20) for the linearized blending operator $F_{\ell,2}^{bqcf,lin}$

$$\begin{aligned} F_{\ell,2}^{bqcf,lin}(u) &= - \left[\left(\frac{\beta_{\ell+k} + 2\beta_\ell + \beta_{\ell-k}}{4} \right) \phi_{xx}(k) \left(\frac{u_{\ell+k} - 2u_\ell + u_{\ell-k}}{a^2} \right) \right. \\ &\quad \left. + \left(1 - \frac{\beta_{\ell+k} + 2\beta_\ell + \beta_{\ell-k}}{4} \right) \phi_{xx}(k) \left(\frac{u_{\ell+1} - 2u_\ell + u_{\ell-1}}{a^2} \right) k^2 \right] \Bigg|_{k=2}, \end{aligned}$$

so, the bilinear form with test function u is

$$\begin{aligned}
\langle F_{,2}^{bqcf,lin}(u), u \rangle &= \sum_{\ell=-M+1}^M F_{\ell,2}^{bqcf,lin}(u) \cdot u_{\ell} a \\
&= \sum_{\ell=-M+1}^M \left\{ - \left(\frac{\beta_{\ell+2} + 2\beta_{\ell} + \beta_{\ell-2}}{4} \right) \phi_{xx}(2) \left(\frac{u_{\ell+2} - 2u_{\ell} + u_{\ell-2}}{a^2} \right) a \right. \\
&\quad \left. - \left(1 - \frac{\beta_{\ell+2} + 2\beta_{\ell} + \beta_{\ell-2}}{4} \right) \phi_{xx}(2) \left(\frac{u_{\ell+1} - 2u_{\ell} + u_{\ell-1}}{a^2} \right) 4a \right\} \cdot u_{\ell}.
\end{aligned} \tag{3.3}$$

We particularly focus on terms contributed to β_{ℓ} as the other terms could be similarly treated. Hence, we divide the constant '1' in (3.3) by $1 = \frac{1}{4} + \frac{2}{4} + \frac{1}{4}$, collect terms contributed to β_{ℓ} and recall the finite difference defined in (2.1), then we have

$$\begin{aligned}
T &:= \frac{-\phi_{xx}(2)}{2} \left[\sum_{\ell=-M+1}^M \left(\frac{u_{\ell+2} - 2u_{\ell} + u_{\ell-2}}{a} \right) (\beta_{\ell} u_{\ell}) + (1 - \beta_{\ell}) \left(\frac{u_{\ell+1} - 2u_{\ell} + u_{\ell-1}}{a} \right) 4u_{\ell} \right] \\
&= \frac{-\phi_{xx}(2)}{2} \left[\sum_{\ell=-M+1}^M \left(u'_{\ell+1} + u'_{\ell} - u'_{\ell-1} - u'_{\ell-2} \right) (\beta_{\ell} u_{\ell}) + (1 - \beta_{\ell}) \left(u'_{\ell} - u'_{\ell-1} \right) 4u_{\ell} \right] \\
&= \frac{-\phi_{xx}(2)}{2} \left[\sum_{\ell=-M+1}^M \left(u'_{\ell} - u'_{\ell-1} \right) 4u_{\ell} \right] \\
&\quad + \frac{-\phi_{xx}(2)}{2} \sum_{\ell=-M+1}^M \left[\left(u'_{\ell+1} - u'_{\ell} \right) - 2 \left(u'_{\ell} - u'_{\ell-1} \right) + \left(u'_{\ell-1} - u'_{\ell-2} \right) \right] \cdot (\beta_{\ell} u_{\ell}) \\
&=: T_1 + T_2.
\end{aligned} \tag{3.4}$$

We consider T_1 first by using Lemma 2.1

$$\begin{aligned}
T_1 &= \sum_{\ell=-M+1}^M \frac{-\phi_{xx}(2)}{2} \left(u'_{\ell} - u'_{\ell-1} \right) 4u_{\ell} = \sum_{\ell=-M+1}^M \frac{\phi_{xx}(2)}{2} u'_{\ell-1} 4 \left(u_{\ell} - u_{\ell-1} \right) \\
&= \sum_{\ell=-M+1}^M \frac{\phi_{xx}(2)}{2} u'_{\ell-1} 4 \left(u'_{\ell-1} \right) a = 2\phi_{xx}(2) \|u'\|_{\ell_2}^2.
\end{aligned} \tag{3.5}$$

Treating T_2 is more tedious and is still mainly based on Lemma 2.1. We have

$$\begin{aligned}
T_2 &= \sum_{\ell=-M+1}^M \frac{-\phi_{xx}(2)}{2} \left[\left(\left(u'_{\ell+1} - u'_{\ell} \right) - \left(u'_{\ell} - u'_{\ell-1} \right) \right) - \left(\left(u'_{\ell} - u'_{\ell-1} \right) - \left(u'_{\ell-1} - u'_{\ell-2} \right) \right) \right] \cdot (\beta_{\ell} u_{\ell}) \\
&= \sum_{\ell=-M+1}^M \frac{\phi_{xx}(2)}{2} \left[\left(\left(u'_{\ell+1} - u'_{\ell} \right) - \left(u'_{\ell} - u'_{\ell-1} \right) \right) \right] \cdot (\beta_{\ell+1} u_{\ell+1} - \beta_{\ell} u_{\ell}) \\
&= \sum_{\ell=-M+1}^M \frac{\phi_{xx}(2)}{2} \left(u''_{\ell} - u''_{\ell-1} \right) a \cdot (\beta_{\ell+1} u_{\ell+1} - \beta_{\ell} u_{\ell}) \\
&= \sum_{\ell=-M+1}^M \frac{-\phi_{xx}(2)}{2} \left(u''_{\ell} \right) a \cdot \left[(\beta_{\ell+1} u_{\ell+1} - \beta_{\ell} u_{\ell}) - (\beta_{\ell} u_{\ell} - \beta_{\ell-1} u_{\ell-1}) \right] \\
&= \sum_{\ell=-M+1}^M \frac{-\phi_{xx}(2)}{2} \left(u''_{\ell} \right) a \cdot \left[(\beta_{\ell+1} u_{\ell+1} - \beta_{\ell} u_{\ell+1}) + (\beta_{\ell} u_{\ell+1} - 2\beta_{\ell} u_{\ell} + \beta_{\ell} u_{\ell-1}) - (\beta_{\ell} u_{\ell-1} - \beta_{\ell-1} u_{\ell-1}) \right] \\
&= \sum_{\ell=-M+1}^M \frac{-\phi_{xx}(2)}{2} \left(u''_{\ell} \right) \cdot \beta_{\ell} u''_{\ell} a^3 + \frac{-\phi_{xx}(2)}{2} \left(u''_{\ell} \right) \cdot \left[\beta'_{\ell} u_{\ell+1} - \beta'_{\ell-1} u_{\ell-1} \right] a^2 \\
&=: -\frac{\phi_{xx}(2)}{2} a^2 \|\sqrt{\beta} u''\|_{\ell_2}^2 + T_{22}.
\end{aligned}$$

Now we mainly focus on T_{22} term, which can be treated as

$$\begin{aligned} T_{22} &= \sum_{\ell=-M+1}^M \frac{-\phi_{xx}(2)}{2} (u'_\ell - u'_{\ell-1}) \cdot [\beta'_\ell u_{\ell+1} - \beta'_{\ell-1} u_{\ell-1}] a \\ &= \sum_{\ell=-M+1}^M \frac{\phi_{xx}(2)}{2} (u'_\ell) \cdot [(\beta'_\ell u_{\ell+1} - \beta'_{\ell-1} u_{\ell-1}) - (\beta'_{\ell-1} u_\ell - \beta'_{\ell-2} u_{\ell-2})] a. \end{aligned}$$

We work on

$$\begin{aligned} &(\beta'_\ell u_{\ell+1} - \beta'_{\ell-1} u_{\ell-1}) - (\beta'_{\ell-1} u_\ell - \beta'_{\ell-2} u_{\ell-2}) \\ &= \beta'_\ell (u_{\ell+1} - u_{\ell-1}) + u_{\ell-1} (\beta'_\ell - 2\beta'_{\ell-1} + \beta'_{\ell-2}) + \beta'_{\ell-1} (u_{\ell-1} - u_\ell) + \beta'_{\ell-2} (u_{\ell-2} - u_{\ell-1}) \\ &= \beta'_\ell (u'_\ell + u'_{\ell-1}) a + u_{\ell-1} \beta_{\ell-1}^{(3)} a^2 - \beta'_{\ell-1} u'_{\ell-1} a - \beta'_{\ell-2} u'_{\ell-2} a. \end{aligned}$$

Then we plug into T_{22} to get

$$\begin{aligned} T_{22} &= \sum_{\ell=-M+1}^M \frac{\phi_{xx}(2)}{2} (u'_\ell) \cdot [\beta'_\ell (u'_\ell + u'_{\ell-1}) a + u_{\ell-1} \beta_{\ell-1}^{(3)} a^2 - \beta'_{\ell-1} u'_{\ell-1} a - \beta'_{\ell-2} u'_{\ell-2} a] a \\ &= \frac{\phi_{xx}(2)}{2} \sum_{\ell=-M+1}^M (u'_\ell) \left([u_{\ell-1} \beta_{\ell-1}^{(3)} a^2 + (\beta'_\ell u'_{\ell-1} - \beta'_{\ell-1} u'_{\ell-1}) a] a + [\beta'_\ell u'_\ell - \beta'_{\ell-2} u'_{\ell-2}] a^2 \right) \\ &= \frac{\phi_{xx}(2)}{2} \sum_{\ell=-M+1}^M \left((u'_\ell) \beta_{\ell-1}^{(3)} (u_{\ell-1}) + (u'_\ell)^2 \beta'_\ell - u''_\ell \beta''_\ell u'_\ell a \right) a^3 \\ &\quad + \frac{\phi_{xx}(2)}{2} \sum_{\ell=-M+1}^M (\beta'_\ell u'_\ell - \beta'_{\ell-2} u'_{\ell-2}) u'_\ell a^2. \end{aligned}$$

Summarizing all terms T_1 , T_2 , T_{22} for terms belong to β_ℓ in (3.3), and treat those for $\beta_{\ell-2}$ and $\beta_{\ell+2}$ in a similar way, we get (3.2) and R , S terms. \square

Remark 3.1. The terms R and S from above are viewed as “residual term”. Thus, we will estimate their bounds controlled by the the support of β'_ℓ , the size of blending region, in pursuit of the positive-definiteness of the bilinear form.

Lemma 3.2. *Let R , S be defined as above, then we have the following estimates*

$$\begin{aligned} |R| &\leq \frac{(-\phi_{xx}(2))}{2} \left(c_3 L^{-\frac{5}{2}} a^{-\frac{1}{2}} + 2c_2 (L)^{-2} \right) \|u'\|_{\ell_2}^2, \\ |S| &\leq (-\phi_{xx}(2)) c_1 (L)^{-1} \|u'\|_{\ell_2}^2, \end{aligned} \tag{3.6}$$

where L is the number of atoms within the blending region Ω_b , $a = \frac{1}{M}$ being the lattice spacing, and $2M$ being the total number of atoms within the periodic domain $\Omega = (-1, 1]$, and the constants c_1 , c_2 and c_3 depend on $\beta^{(j)}$ with $j = 1, \dots, 3$, respectively.

Proof. Recall that

$$R = \sum_{\ell=-M+1}^M \frac{\phi_{xx}(2)}{2} (u'_\ell \beta_{\ell-1}^{(3)} (u_{\ell-1}) - u''_\ell \beta''_\ell u'_\ell a) a^3.$$

Also notice that the finite differences of β are nonzero only on Ω_b , so utilizing the fact that $\phi_{xx}(2) \leq 0$ and Hölder’s Inequality, we get

$$\begin{aligned} |R| &\leq \left| \sum_{\ell \in \Omega^b} \frac{\phi_{xx}(2)}{2} (u'_\ell) (\beta_{\ell-1}^{(3)} (u_{\ell-1})) a^3 \right| + \left| \sum_{\ell \in \Omega^b} \frac{\phi_{xx}(2)}{2} u''_\ell \beta''_\ell u'_\ell a^4 \right| \\ &\leq \frac{-\phi_{xx}(2)}{2} \|\beta^{(3)}\|_{\ell^\infty} \|u'\|_{\ell_2(\Omega^b)} \|u\|_{\ell_2(\Omega^b)} a^2 + \frac{-\phi_{xx}(2)}{2} \|\beta^{(2)}\|_{\ell^\infty} \|u''\|_{\ell_2(\Omega^b)} \|u'\|_{\ell_2(\Omega^b)} a^3. \end{aligned}$$

Also notice that $|\Omega_b| = La$ and by the discrete Poincaré Inequality, we have $\|u\|_{\ell_2(\Omega^b)} \leq (La)^{\frac{1}{2}} \|u'\|_{\ell_2}$. In addition, we use the fact that $\|\beta^{(j)}\|_{\ell^\infty} \leq c(La)^{-j}$. Then

$$\begin{aligned} |R| &\leq \frac{-\phi_{xx}(2)}{2} \|\beta^{(3)}\|_{\ell^\infty} \|u'\|_{\ell_2(\Omega^b)} \|u\|_{\ell_2(\Omega^b)} a^2 + \frac{-\phi_{xx}(2)}{2} \|\beta^{(2)}\|_{\ell^\infty} \|u''\|_{\ell_2(\Omega^b)} \|u'\|_{\ell_2(\Omega^b)} a^3 \\ &\leq \frac{-\phi_{xx}(2)}{2} c_3 (La)^{-3} (La)^{\frac{1}{2}} \|u'\|_{\ell_2}^2 a^2 + \frac{-\phi_{xx}(2)}{2} c_2 (La)^{-2} \frac{2}{a} \|u'\|_{\ell_2}^2 a^3 \\ &\leq \frac{-\phi_{xx}(2)}{2} \left(c_3 L^{-\frac{5}{2}} a^{-\frac{1}{2}} + 2c_2 (L)^{-2} \right) \|u'\|_{\ell_2}^2. \end{aligned}$$

Next, we bound S . Recall that

$$S := \sum_{\ell=-M+1}^M \frac{\phi_{xx}(2)}{2} (u'_\ell)^2 a^2 \left(\beta'_\ell u'_\ell - \beta'_{\ell-2} u'_{\ell-2} \right).$$

Utilizing similar inequalities, we obtain

$$|S| \leq \frac{-\phi_{xx}(2)}{2} \|\beta'\|_{\ell^\infty} \cdot 2 \|u'\|_{\ell_2}^2 a \leq \frac{-\phi_{xx}(2)}{2} c_1 (La)^{-1} \cdot 2 \|u'\|_{\ell_2}^2 a = \left(-\phi_{xx}(2) \right) c_1 (L)^{-1} \|u'\|_{\ell_2}^2.$$

Hence, we prove the lemma. \square

Theorem 3.1. *Suppose that the number of atoms M within the chain model is sufficiently large, or equivalently the lattice spacing $a = \frac{1}{M}$ is sufficiently small; also suppose that the fully atomistic model with next-nearest-neighbor interaction $N = 2$, is stable so that $[\phi_{xx}(1) + 4\phi_{xx}(2)] > 0$. Let L denote the number of atoms within the blending region and let the blending function β be sufficiently smooth such that $\|\beta^{(j)}\|_{\ell^\infty} \leq (La)^{-j}$. Then there exists a positive constant \tilde{C} such that*

$$\sum_{k=1}^2 \sum_{\ell=-M+1}^M \langle F_{\ell,k}^{bqcf,lin} u, u \rangle \geq \tilde{C} \|u'\|_{\ell_2}^2 \quad (3.7)$$

\tilde{C} is strictly bounded above zero as $a = \frac{1}{M} \rightarrow 0$.

Proof. For $N = 2$ and from Lemma 3.1, the blended force-based operator satisfies

$$\begin{aligned} \sum_{\ell=-M+1}^M \langle F_{\ell,2}^{bqcf,lin}(u), u \rangle &= (\phi_{xx}(1) + 4\phi_{xx}(2)) \|u'\|_{\ell_2}^2 - \phi_{xx}(2) a^2 \left\| \sqrt{\beta} u'' \right\|_{\ell_2}^2 + \phi_{xx}(2) a^2 \left\| \sqrt{\beta''} u' \right\|_{\ell_2}^2 \\ &\quad + 2R + 2S. \end{aligned} \quad (3.8)$$

From Lemma 3.2, we have

$$\begin{aligned} |2R + 2S| &\leq -\frac{\phi_{xx}(2)}{2} \left(2c_3 L^{-\frac{5}{2}} a^{-\frac{1}{2}} + 4c_2 L^{-2} + c_1 L^{-1} \right) \|u'\|_{\ell_2}^2 \\ &\leq -\frac{\phi_{xx}(2)}{2} \left(c_4 L^{-\frac{5}{2}} a^{-\frac{1}{2}} \right) \|u'\|_{\ell_2}^2, \end{aligned} \quad (3.9)$$

hence, we have

$$2R + 2S \geq \frac{\phi_{xx}(2)}{2} \left(c_4 L^{-\frac{5}{2}} a^{-\frac{1}{2}} \right) \|u'\|_{\ell_2}^2$$

with the latter inequality following from $L^{-2} \leq L^{-1} \leq L^{-\frac{5}{2}} a^{-\frac{1}{2}}$ as $L^{-\frac{5}{2}} a^{-\frac{1}{2}}$ dominates the latter two terms when a is sufficiently small.

From (3.8), we want to observe the terms that do not favor the coercivity in the terms of the H^1 semi-norm. For the second term, since $\phi_{xx}(2) \leq 0$, we have

$$-\phi_{xx}(2) a^2 \left\| \sqrt{\beta} u'' \right\|_{\ell_2}^2 \geq 0,$$

and thus it does not negatively contribute. For the third term we observe that

$$\phi_{xx}(2)a^2 \left\| \sqrt{\beta''} u' \right\|_{\ell_2}^2 \geq \phi_{xx}(2)c_5L^{-2} \|u'\|_{\ell_2}^2$$

because of $\phi_{xx}(2) \leq 0$. For up to $N = 2$ neighbour interaction, we have from the coercivity of atomistic model that $\phi''(1) + 4\phi''(2) > 0$, hence, for the linearized force-blended model, we have

$$\langle F_{,1}^{bqcf,lin} + F_{,2}^{bqcf,lin}, u \rangle \geq \left[\phi_{xx}(1) + \phi_{xx}(2) \left(4 + c_4L^{-\frac{5}{2}}a^{-\frac{1}{2}} + c_5L^{-2} \right) \right] \|u'\|_{\ell_2}^2 \geq \tilde{C} \|u'\|_{\ell_2}^2$$

for $\tilde{C} = (\phi_{xx}(1) + 2\phi_{xx}(2)) > 0$ strictly positive, and independent of $a \rightarrow 0$.

Thus, we can conclude that the necessary and optimal blending size for coercivity is $L^{-\frac{5}{2}}a^{-\frac{1}{2}} \lesssim 1/c_4$ that is $L = \hat{C}a^{-\frac{1}{5}} = \hat{C}M^{\frac{1}{5}}$ for some $\hat{C} > 0$. \square

3.3 Stability Analysis for general N -th Nearest Neighbor Interaction Range

To observe the general form of the N -th neighbor interaction range, we notice that for $k = 3, \dots, N$

$$\begin{aligned} \langle F_{,k}^{bqcf,lin}(u), u \rangle &= -\phi_{xx}(k) \sum_{\ell=-M+1}^M \left\{ \left(\frac{\beta_{\ell+k} + 2\beta_{\ell} + \beta_{\ell-k}}{4} \right) \left(\frac{u_{\ell+k} - 2u_{\ell} + u_{\ell-k}}{a^2} \right) \right. \\ &\quad \left. + \left(1 - \frac{\beta_{\ell+k} + 2\beta_{\ell} + \beta_{\ell-k}}{4} \right) k^2 \left(\frac{u_{\ell+1} - 2u_{\ell} + u_{\ell-1}}{a^2} \right) \right\} u_{\ell} a. \end{aligned} \quad (3.10)$$

The k -th neighbor interaction differs by having $\beta_{\ell \pm k}$ terms which are treated similarly to β_{ℓ} terms. $\phi_{xx}(k)$ is a non-positive constant term for all $k \geq 2$.

Similarly to the previous subsection, we fix an interaction range k and at the moment only consider all terms that contribute to β_{ℓ} , thus we get

$$\begin{aligned} T &:= -\frac{\phi_{xx}(k)}{2} \sum_{\ell=-M+1}^M \left(k^2 \frac{u_{\ell+1} - 2u_{\ell} + u_{\ell-1}}{a} \right) (u_{\ell}) \\ &\quad - \frac{\phi_{xx}(k)}{2} \sum_{\ell=-M+1}^M \left[\left(\frac{u_{\ell+k} - 2u_{\ell} + u_{\ell-k}}{a} - k^2 \frac{u_{\ell+1} - 2u_{\ell} + u_{\ell-1}}{a} \right) (\beta_{\ell} u_{\ell}) \right] \\ &= T_1 + T_2. \end{aligned}$$

For T_1 , we similarly have

$$\begin{aligned} T_1 &= -\frac{\phi_{xx}(k)}{2} \sum_{\ell=-M+1}^M \left(k^2 \frac{u_{\ell+1} - 2u_{\ell} + u_{\ell-1}}{a} \right) (u_{\ell}) \\ &= -\frac{\phi_{xx}(k)}{2} \sum_{\ell=-M+1}^M k^2 (u'_{\ell} - u'_{\ell-1}) u_{\ell} = \frac{k^2}{2} \phi_{xx}(k) \|u'\|_{\ell_2}^2. \end{aligned} \quad (3.11)$$

For T_2 , the simplification is more difficult, we have

$$\begin{aligned}
T_2 &= -\frac{\phi_{xx}(k)}{2} \sum_{\ell=-M+1}^M \left[\left(\frac{u_{\ell+k} - 2u_\ell + u_{\ell-k}}{a} - k^2 \frac{u_{\ell+1} - 2u_\ell + u_{\ell-1}}{a} \right) (\beta_\ell u_\ell) \right] \\
&= -\frac{\phi_{xx}(k)}{2} \sum_{\ell=-M+1}^M \left[\left(\sum_{j=1}^k \sum_{s=1}^k u''_{\ell-j+s} \right) - k^2 u''_\ell \right] (a\beta_\ell u_\ell) \\
&= -\frac{\phi_{xx}(k)}{2} \sum_{\ell=-M+1}^M \left[\sum_{j=1}^k \sum_{s=1}^k \left(u''_{\ell-j+s} - u''_\ell \right) \right] (a\beta_\ell u_\ell).
\end{aligned}$$

Due to the exact symmetry of j and s , we have

$$\sum_{j=1}^k \sum_{s=1}^k u''_{\ell-j+s} = \sum_{j=1}^k \sum_{s=1}^k u''_{\ell-s+j}.$$

Hence, T_2 can be converted into a symmetrical form

$$\begin{aligned}
T_2 &= -\frac{\phi_{xx}(k)}{2} \sum_{\ell=-M+1}^M \left[\sum_{j=1}^k \sum_{s=1}^k \left(u''_{\ell-j+s} - u''_\ell \right) \right] (a\beta_\ell u_\ell) \\
&= -\frac{\phi_{xx}(k)}{4} \sum_{\ell=-M+1}^M \left[\sum_{j=1}^k \sum_{s=1}^k \left(u''_{\ell-j+s} - 2u''_\ell + u''_{\ell+j-s} \right) \right] (a\beta_\ell u_\ell) \\
&= -\frac{\phi_{xx}(k)}{4} \sum_{\ell=-M+1}^M \left[\sum_{j=1}^k \sum_{s=1}^k \left(u''_{\ell-j+s} - u''_\ell \right) - \left(u''_\ell - u''_{\ell+j-s} \right) \right] (a\beta_\ell u_\ell).
\end{aligned} \tag{3.12}$$

Therefore by the discrete summation by parts formula, we have

$$\begin{aligned}
T_2 &= \frac{\phi_{xx}(k)}{4} \sum_{\ell=-M+1}^M \left[\sum_{j=1}^k \sum_{s=1}^k \left(u''_{\ell-j+s} - u''_\ell \right) \right] a \left(\beta_{\ell-j+s} u_{\ell-j+s} - \beta_\ell u_\ell \right) \\
&= \frac{-\phi_{xx}(k)}{4} \sum_{\ell=-M+1}^M \left[\sum_{j=1}^k \sum_{s=1}^k u''_\ell a \right] \left(\left(\beta_{\ell-j+s} u_{\ell-j+s} - \beta_\ell u_\ell \right) - \left(\beta_\ell u_\ell - \beta_{\ell+j-s} u_{\ell+j-s} \right) \right) \\
&= \frac{-\phi_{xx}(k)}{4} \sum_{\ell=-M+1}^M \left[\sum_{j=1}^k \sum_{s=1}^k u''_\ell a \right] \left(\beta_{\ell-j+s} u_{\ell-j+s} - 2\beta_\ell u_\ell + \beta_{\ell+j-s} u_{\ell+j-s} \right).
\end{aligned} \tag{3.13}$$

We can carefully work on the symmetrical term

$$\begin{aligned}
&\left(\beta_{\ell-j+s} u_{\ell-j+s} - 2\beta_\ell u_\ell + \beta_{\ell+j-s} u_{\ell+j-s} \right) \stackrel{r:=j-s}{=} \left(\beta_{\ell-r} u_{\ell-r} - 2\beta_\ell u_\ell + \beta_{\ell+r} u_{\ell+r} \right) \\
&= \beta_{\ell-r} u_{\ell-r} - \beta_\ell u_{\ell+1} + \left(\beta_\ell u_{\ell+1} - 2\beta_\ell u_\ell + \beta_\ell u_{\ell-1} \right) - \beta_\ell u_{\ell-1} + \beta_{\ell+r} u_{\ell+r} \\
&= \beta_\ell u''_\ell a^2 + \beta_{\ell-r} u_{\ell-r} - \beta_\ell u_{\ell+1} + \beta_{\ell+r} u_{\ell+r} - \beta_\ell u_{\ell-1}.
\end{aligned}$$

Without loss of generality, we assume $r > 0$, then

$$\begin{aligned}
&\left(\beta_{\ell-r} u_{\ell-r} - 2\beta_\ell u_\ell + \beta_{\ell+r} u_{\ell+r} \right) = \beta_\ell u''_\ell a^2 + \beta_{\ell-r} u_{\ell-r} - \beta_\ell u_{\ell+1} + \beta_{\ell+r} u_{\ell+r} - \beta_\ell u_{\ell-1} \\
&= \beta_\ell u''_\ell a^2 + \left(\beta_\ell u_{\ell-r} - \beta_\ell u_{\ell-1} \right) + \left(\beta_\ell u_{\ell+r} - \beta_\ell u_{\ell+1} \right) + u_{\ell+r} \sum_{t=0}^{r-1} \beta'_{\ell+t} a - u_{\ell-r} \sum_{t=0}^{r-1} \beta'_{\ell-r+t} a.
\end{aligned} \tag{3.14}$$

Therefore, we can handle T_2 for general k -th-neighbor-interaction range in a similar way to that for the case of $k = 2$, and obtain that

$$|T_2| \leq (-\phi_{xx}(k)) \left(|\tilde{c}_4| L^{-\frac{5}{2}} a^{-\frac{1}{2}} + |\tilde{c}_5| L^{-2} \right) \|u'\|_{\ell_2}^2$$

which suggests that for $k \geq 2$

$$T_2 \geq (\phi_{xx}(k)) \left(\tilde{c}_4 L^{-\frac{5}{2}} a^{-\frac{1}{2}} + \tilde{c}_5 L^{-2} \right) \|u'\|_{\ell_2}^2.$$

Combining with T_1 estimate (3.11), we have for any $k \geq 2$

$$\langle F_{,k}^{bqcf,lin}(u), u \rangle \geq \phi_{xx}(k) \left(k^2 + \hat{C}_k L^{-\frac{5}{2}} a^{-\frac{1}{2}} + \hat{C}_k L^{-2} \right) \|u'\|_{\ell_2}^2 \quad (3.15)$$

with $L = \tilde{C} a^{-\frac{1}{5}}$ when $a = \frac{1}{M}$ being sufficiently small.

Thus, collecting all interactions up to the N -th Nearest Neighbor Interaction Range, we have

$$\begin{aligned} \langle F_{,k}^{bqcf,lin}(u), u \rangle &= \langle F_{,1}^{bqcf,lin}(u), u \rangle + \sum_{k=2}^N \langle F_{,k}^{bqcf,lin}(u), u \rangle \\ &\geq \left[\phi_{xx}(1) + \sum_{k=2}^N \phi_{xx}(k) \left(k^2 + \hat{C}_k L^{-\frac{5}{2}} a^{-\frac{1}{2}} \right) \right] \|u'\|_{\ell_2}^2. \end{aligned}$$

Hence, similar to Theorem 3.1, we summarize the stability conditions on the blending size for a general atomistic chain with N -th Nearest Neighbour interaction in the following theorem.

Theorem 3.2. *Suppose that the number of atoms M is sufficiently large, which is equivalent to $a = \frac{1}{M}$ being sufficiently small, and the blending function β is sufficiently smooth. Also, we assume that the fully atomistic model is stable so that*

$$\left[\phi_{xx}(1) + \sum_{k=1}^N k^2 \phi_{xx}(k) \right] > 0.$$

If the blending size L satisfies $L = \tilde{C} a^{-\frac{1}{5}}$, then the linear B-QCF operator $F_{,k}^{bqcf,lin}$ is positive-definite in terms of the H^1 semi-norm

$$\sum_{k=1}^N \sum_{\ell=-M+1}^M \langle F_{\ell,k}^{bqcf,lin} u, u \rangle \geq \tilde{C} \|u'\|_{\ell_2}^2, \quad (3.16)$$

where \tilde{C} is strictly bounded above zero as $a = \frac{1}{M} \rightarrow 0$.

Meanwhile, we can see that the bounds are dependent on the smoothness of β . Therefore, we aim to find the optimal types of blending function to preserve the bounds in the coming numerical session.

Remark 3.2. Throughout, the term ‘optimal’ is used to describe the conclusion that $L = \tilde{C} a^{-\frac{1}{5}}$ is the optimal blending size for keeping coercivity of the force operator when $a = \frac{1}{M} \rightarrow 0$. Optimality in these instances describes the smallest asymptotic order that could be expected to ensure stability. However, the analysis of consistency conditions is beyond the purview of this paper. Note that \hat{C} is dependent on the blending function, β , and the choice for potential energy, ϕ ; and it is not on the lattice spacing constant, a .

Also notice from the inequality (3.15) that $\hat{C}_k L^{-\frac{5}{2}} a^{-\frac{1}{2}}$ dominates the other terms only when the lattice spacing $a = \frac{1}{M}$ is very small. As a result, the asymptotically rate $L \sim a^{-\frac{1}{5}} = M^{\frac{1}{5}}$ might be not observed when the size of atomistic chain is only moderately large. In this case, we suggest to take $L \sim a^{-\frac{1}{5}} = M^{\frac{1}{5}}$, which is observed in the numerical test.

4 Numerical Experiments

We conduct numerical experiments to verify the theoretical findings from the stability analysis.

4.1 Blending Size and the Stability Constant

We consider a periodic chain with atom indices from $-M + 1$ to M . For the following numerical simulations, we set $M = 2000$. The optimal blending size as was found analytically in the previous section is $M^{1/5} \approx 5$. We will test to see if the numerical experiments coincide with this value.

First, we apply the uniform stretch to the atomistic chain and compute the critical strain when $F^{a,lin}$ and $F^{bqc,lin}$ loses the coercivity. We compare the critical strain values between the atomistic model and blending models with different blending sizes and various types of blending functions. By comparing these values to the atomistic critical strain error, we obtain the optimal blending function and attempt to verify the optimal blending size of $M^{1/5}$ found before.

In numerical experiments, the Morse Potential,

$$\phi(r) = D_e \times [1 - e^{-\alpha(r-r_e)}]^2,$$

was utilized for the interaction potential due to its popularity in applications. We use the values $D_e = 3$ and $\alpha = 3, 4, \text{ and } 5$, respectively. Recall from Figure 1, the local minimal value is set to be $\phi(1)$ and the local height of the potential is D_e . Also, as α grows larger, the more narrow the potential becomes.

We will consider our computational domain as $\Omega = (-1, 1]$ with periodic boundary conditions. The computational domain will be decomposed into several sub-domains following [13]. An interaction range is introduced to serve as a buffer region to simplify the treatment of periodic boundary conditions. The lattice spacing constant that was used had a value of $a = \frac{1}{M}$ which helped to start the blending region.

For the numerical experiments, we denote the blending region, $\Omega^b = (b_1, b_2)$ for some $b_1, b_2 \in \Omega$. The numerical blending size, L , will be defined as $L = b_2 - b_1$. We can compare the numerical blending size to that which was found in the stability analysis.

Recall from Definition (2.18),

$$\beta(x) = \begin{cases} 1, & x \in \Omega^a \\ 0, & x \in \Omega^c \\ \in (0, 1), & x \in \Omega^b = (b_1, b_2). \end{cases}$$

We conduct numerical experiments using a piecewise linear spline, piecewise cubic spline, and piecewise quintic spline blending function which are defined as follows:

$$\beta^{linear}(x) := \begin{cases} 1, & x \in \Omega^a, \\ 0, & x \in \Omega^c, \\ 1 - \frac{x-b_1}{L}, & x \in \Omega^b, \end{cases}$$

and

$$\beta^{cubic}(x) := \begin{cases} 1, & x \in \Omega^a, \\ 0, & x \in \Omega^c, \\ 1 + 2\left(\frac{x-b_1}{L}\right)^3 - 3\left(\frac{x-b_1}{L}\right)^2, & x \in \Omega^b, \end{cases}$$

and

$$\beta^{quintic}(x) := \begin{cases} 1, & x \in \Omega^a, \\ 0, & x \in \Omega^c, \\ 1 - 6\left(\frac{x-b_1}{L}\right)^5 + 15\left(\frac{x-b_1}{L}\right)^4 - 10\left(\frac{x-b_1}{L}\right)^3, & x \in \Omega^b. \end{cases}$$

Graphical demonstrations of these various blending functions can be found in Figure 2.

We apply a uniform stretch to the atomistic chain. From this, we numerically compute the critical strains of the atomistic model and compare this to the coupling model with different blending sizes in pursuit of the critical stretch value that makes the atomistic chain unstable. The step size for increasing γ is $\Delta\gamma = 10^{-5}$. We also model the different values of α in the Morse Potential using the cubic blending function. As can

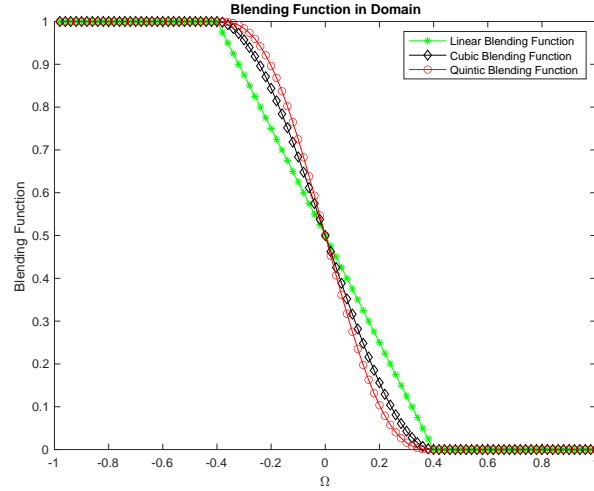


Figure 2: Pictorial representation of the blending functions used in numerical experiments. Recall, at $\beta = 1$, the purely atomistic model is obtained and at $\beta = 0$, the purely continuum model is obtained.

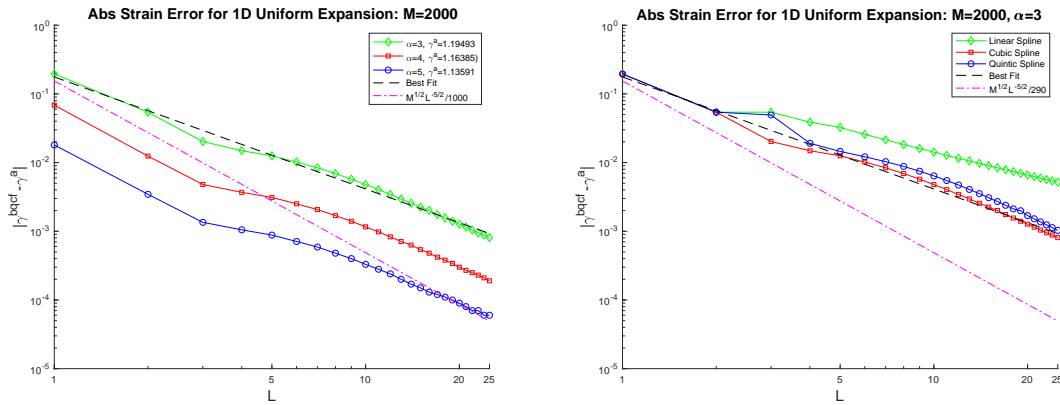


Figure 3: The absolute critical strain errors are plotted for the 1D uniform stretching. We set $M=2,000$ and γ^a and γ^{bqcf} are the critical strains for the atomistic and B-QCF models, respectively. a) Models the cubic spline blending for various values of α ; and b) models the critical strain errors of linear, cubic, and quintic blending functions with $M = 2,000$ and $\alpha = 3$.

Blend size	Linear	Cubic	Quintic
1	1	1	1
2	1.1400	1.1409	1.1409
3	1.1269	1.1747	1.1456
4	1.1562	1.1801	1.1759
5	1.1624	1.1824	1.1804
6	1.1692	1.1848	1.1828
7	1.1735	1.1866	1.1847
10	1.1811	1.1950	1.1950

Table 1: Shown are the critical stretching values for linear, cubic, and quintic blending models for a blending size from a to $10a$. The critical value for the purely atomistic model was found to be $\gamma^a = 1.195$. The numerical increment for $\Delta\gamma$ is 10^{-5} .

be seen in Table 1, the cubic blending function reaches the atomistic critical stretch value quicker than the other two blending functions.

The results from Table 1 suggest the blending size to be $L \approx M^{\frac{1}{3}}$, this might be due to the other terms in the inequality (3.15) when observing only a moderately large atomistic chain. For further clarification, see Remark 4.1.

The results from the numerical experiments find the cubic blending function as that which converges quickest toward the atomistic strain value and is thus the optimal blending function from those we tested.

Remark 4.1. Recall from (3.9), the assumption that:

$$\left(2c_3L^{-\frac{5}{2}}a^{-\frac{1}{2}} + 4c_2L^{-2} + c_1L^{-1}\right) \leq \left(c_4L^{-\frac{5}{2}}a^{-\frac{1}{2}}\right).$$

The latter two terms on the left side of the inequality would not necessarily be negligible if the number of atoms M were not large enough. This accounts for the difference observed in the blending size between the analysis and the numerical simulation.

It must be noted that the analysis conducted in the previous section only applies to the cubic or quintic blending function used in these simulations. Due to less regularities near the boundaries of the blending region, the analysis does not encompass the linear blending function. In these experiments, we can also see that the linear blending leads to the most discrepancies.

4.2 Simulation of Deformed Configuration

Now that we found that the cubic blending function as the optimal blending function, we utilize this for the remaining numerical tests. We use a blend size $L = 5$ since $2000^{\frac{1}{3}} \approx 4.57$ as well as $\alpha = 3$ for both numerical experiments. Next, we test two functions with periodic boundary conditions as the external force of the system to ensure the blended coupling scheme performs as imagined.

- **First, we use a sinusoidal external force**

$$F_{\ell}^{ext} = 0.01a \times \sin(-x_{\ell} \times \pi).$$

We use $a = \frac{1}{5}$ numerically and incorporate -1 into sine because of our left domain boundary.

We obtain the expected force plot for our domain as can be seen in 4. The displacement is also observed for an interaction range potential from first neighbor up to third neighbor. We observe that the difference between an interaction range potential of $N = 2$ versus an interaction range potential of $N = 3$ is much smaller than the difference between the change in displacement for the interaction range potential for $N = 1$ and $N = 2$. Recall, the features of the Morse Potential are such that $\phi_{xx}(1) > 0$ and $\phi_{xx}(k) \leq 0$ for $k \geq 2$. Thus, after the next-nearest neighbor, $k = 2$, the change in displacement will not differ by as much.

- **Next, we test a Gaussian external force:**

$$F_{\ell}^{ext} = 0.01 \times a \times e^{-\frac{(x_{\ell}-\mu)^2}{2\sigma^2}},$$

where $\mu = 4a$, $\sigma = 50a$, and $a = 1/M$ with $M = 2000$ was used.

Again, we show the force output for our domain and show the various displacements for three interaction range potentials. Similarly to the sinusoidal external force, once the interaction range reaches a value of $N = 2$, the change in displacement becomes less significant.

5 Conclusion

In this paper, inspired by the force-based coupling of the peridynamics model of [13], we have formulated a similar symmetric and consistent blended force-based atomistic-to-continuum coupling scheme in one-dimensional space. We were able to identify the optimal asymptotic conditions on the width of the blending region, $L \approx M^{\frac{1}{3}}$ to ensure the H^1 stability of the linearized force-blending operator when chain size is huge.

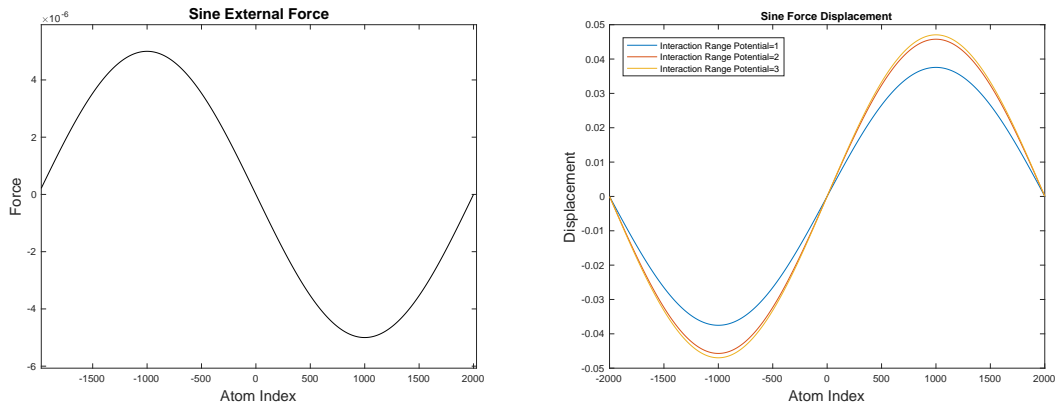


Figure 4: a) A sinusoidal external force is shown. b) The various displacements for this external force are displayed within the domain.

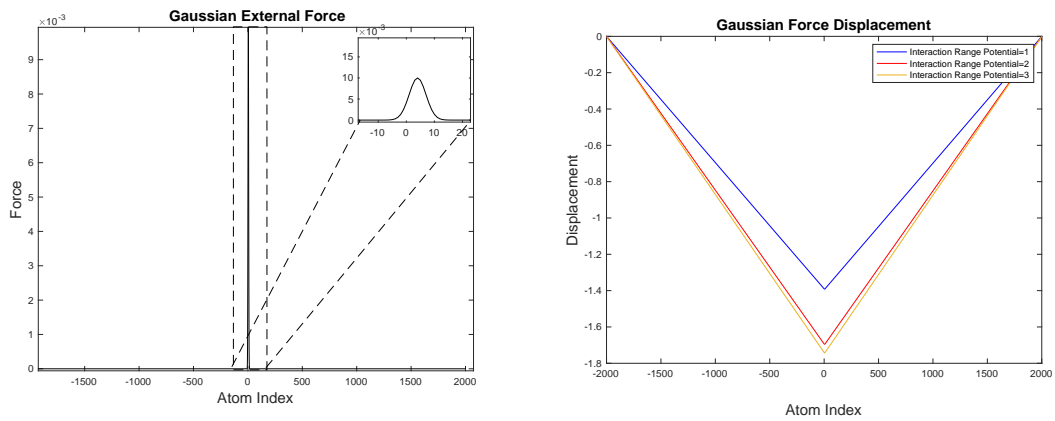


Figure 5: a) A Gaussian external force is shown. b) The various displacement for this external force are displayed within the domain.

We have verified the theoretical findings with numerical experiments on the blending function and the blending region. From these numerical experiments, we find that the cubic blending provides the best results compared to the critical stretch of the fully atomistic model. We also find that the optimal blending width from these numerical experiments is $L \approx M^{\frac{1}{3}}$ due to non-negligible terms when *not working with* a large enough atomistic chain.

In the future, extension of this scheme to two-dimensional atomistic-to-continuum coupling with a triangular crystal lattice in regards to the neighbors will be pursued.

6 Acknowledgements

Elaine Gorom-Alexander and Dr. X. Li are supported by NSF CAREER award: DMS-1847770 and the University of North Carolina at Charlotte Faculty Research Grant.

We would like to thank the helpful discussions from Dr. Pablo Seleson and Dr. Christoph Ortner. We also want to thank the opportunity provided by the 50th John H. Barrett Memorial Lectures organizing committee.

7 Appendix

7.1 A More Rigorous Proof for Proposition 2.2, A Consistency Analysis of Force

Proof. Comparing $F_{\ell}^{c,lin}$ and $F_{\ell}^{a,lin}$, we have

$$F_{\ell}^{c,lin}(u) - F_{\ell}^{a,lin}(u) = - \sum_{\substack{k=-N, \\ k \neq 0}}^N \frac{1}{2} \phi_{xx}(k) (k^2 u_{\ell}'') + \sum_{\substack{k=-N, \\ k \neq 0}}^N \frac{1}{2} \phi_{xx}(k) \left(\frac{u_{\ell+k} - 2u_{\ell} + u_{\ell-k}}{a^2} \right).$$

Let $N \in \mathbb{N}$ be fixed. For any $k = -N, \dots, N$ and $k \neq 0$, we apply the Taylor expansion to $\tilde{u}_{\ell+k} = u_{\ell+k}$ and $\tilde{u}_{\ell-k} = u_{\ell-k}$ around ℓ . We compare the differencing notation used to define the discrete displacement field with choosing a smooth spline interpolation. We proceed with defining \tilde{u}_x as this smooth interpolation of the discrete displacement field u in order to compute this approximation.

$$\begin{aligned} u_{\ell+k} &= u_{\ell} + ka\tilde{u}_x + \frac{1}{2}(ka)^2\tilde{u}_{xx} + \frac{1}{6}(ka)^3\tilde{u}_{xxx} + O(a^4), \\ u_{\ell-k} &= u_{\ell} - ka\tilde{u}_x + \frac{1}{2}(ka)^2\tilde{u}_{xx} - \frac{1}{6}(ka)^3\tilde{u}_{xxx} + O(a^4). \end{aligned}$$

Thus, for all k ,

$$\begin{aligned} u_{\ell+k} - 2u_{\ell} + u_{\ell-k} &= u_{\ell} + ka\tilde{u}_x + \frac{1}{2}(ka)^2\tilde{u}_{xx} + \frac{1}{6}(ka)^3\tilde{u}_{xxx} + O(a^4) - 2u_{\ell} \\ &\quad + u_{\ell} - ka\tilde{u}_x + \frac{1}{2}(ka)^2\tilde{u}_{xx} - \frac{1}{6}(ka)^3\tilde{u}_{xxx} + O(a^4) \\ &= (ka)^2\tilde{u}_{xx} + O(a^4). \end{aligned} \tag{7.1}$$

Utilizing (7.1) for the atomistic and continuous force equations, the consistency analysis yields:

$$\begin{aligned}
& F_{\ell}^{c,lin}(u) - F_{\ell}^{a,lin}(u) \\
&= - \sum_{\substack{k=-N, \\ k \neq 0}}^N \frac{1}{2} \phi_{xx}(k) (k^2 u_{\ell}'') + \sum_{\substack{k=-N, \\ k \neq 0}}^N \frac{1}{2} \phi_{xx}(k) \left(\frac{u_{\ell+k} - 2u_{\ell} + u_{\ell-k}}{a^2} \right) \\
&= - \sum_{\substack{k=-N, \\ k \neq 0}}^N \frac{1}{2} k^2 \phi_{xx}(k) \left(\frac{u_{\ell+1} - 2u_{\ell} + u_{\ell-1}}{a^2} \right) + \sum_{\substack{k=-N, \\ k \neq 0}}^N \frac{1}{2} \phi_{xx}(k) \left(\frac{u_{\ell+k} - 2u_{\ell} + u_{\ell-k}}{a^2} \right) \\
&= - \sum_{\substack{k=-N, \\ k \neq 0}}^N \frac{1}{2} k^2 \phi_{xx}(k) \frac{a^2 \tilde{u}_{xx} + O(a^4)}{a^2} + \sum_{\substack{k=-N, \\ k \neq 0}}^N \frac{1}{2} k^2 \phi_{xx}(k) \frac{(ka)^2 \tilde{u}_{xx} + O(a^4)}{a^2} \\
&= - \sum_{\substack{k=-N, \\ k \neq 0}}^N \frac{1}{2} k^2 \phi_{xx}(k) \tilde{u}_{xx} + \sum_{\substack{k=-N, \\ k \neq 0}}^N \frac{1}{2} k^2 \phi_{xx}(k) \tilde{u}_{xx} + O(a^2) \\
&= O(a^2).
\end{aligned}$$

Thus, the consistency error between the linearized atomistic force equation and the continuum force equation is $O(a^2)$. \square

7.2 Analysis in the continuous setting

Before finding the nearest neighbor and the next-nearest neighbor interaction for the discrete case, the continuous case was observed. The continuous case was meant to shed light on the nature of the discrete case as it would be easier to find.

From (2.20) we look at the next-nearest neighbor interaction. Also, we will approximate $\frac{\beta_{\ell+k} + 2\beta_{\ell} + \beta_{\ell-k}}{4} \approx \beta(x_{\ell})$. Thus, (2.20) becomes for the force-based operator:

$$\begin{aligned}
F_{\ell}^{bqcf,lin} &= \left(\frac{\beta_{\ell-1} + 2\beta_{\ell} + \beta_{\ell+1}}{4} \right) \phi_{xx}(1) \left(\frac{u_{\ell+1} - 2u_{\ell} + u_{\ell-1}}{a^2} \right) + \left(1 - \frac{\beta_{\ell-1} + 2\beta_{\ell} + \beta_{\ell+1}}{4} \right) \phi_{xx}(1) u_{\ell}'' \\
&+ \left(\frac{\beta_{\ell-2} + 2\beta_{\ell} + \beta_{\ell+2}}{4} \right) \phi_{xx}(2) \left(\frac{u_{\ell+2} - 2u_{\ell} + u_{\ell-2}}{a^2} \right) + \left(1 - \frac{\beta_{\ell-2} + 2\beta_{\ell} + \beta_{\ell+2}}{4} \right) \phi_{xx}(2) 4u_{\ell}'' \\
&\approx \beta(x_{\ell}) \left(\phi_{xx}(1) u_{\ell}'' + \phi_{xx}(2) \left(\frac{u_{\ell+2} - 2u_{\ell} + u_{\ell-2}}{a^2} \right) \right) + (1 - \beta(x_{\ell})) \left(\phi_{xx}(1) u_{\ell}'' + 4\phi_{xx}(2) u_{\ell}'' \right).
\end{aligned}$$

Using a Taylor approximation on $u_{\ell+2}$ and $u_{\ell-2}$, the next-nearest neighbor operator becomes

$$F_{\ell}^{bqcf,lin} = \phi_{xx}(1) u_{\ell}'' + \beta(x_{\ell}) \phi_{xx}(2) \left(4u_{\ell}'' + \frac{4}{3} u_{\ell}^{(4)} a^2 \right) + (1 - \beta(x_{\ell})) 4\phi_{xx}(2) u_{\ell}''. \quad (7.2)$$

Since the nearest neighbor interaction is not difficult to find, we drop it from the continuous case to find the approximation for the next-nearest neighbor as well as utilize the fact that ϕ is a Lennard Jones type potential. Also, we denote $\beta(x_{\ell})$ by β when there is no ambiguity. Therefore, the continuous next-nearest operator becomes

$$\begin{aligned}
Fu_x &= \beta(-u_{xx} + a^2 Au_{xxxx}) + (1 - \beta)(-u_{xx}) \\
&= \beta a^2 Au_{xxxx} - u_{xx}
\end{aligned} \quad (7.3)$$

where $A = \frac{4}{3}$.

Lemma 7.1. For any displacements $u = (u_\ell)_{\ell \in \mathbb{Z}}$ from y_ℓ , the nearest neighbor and the next-nearest neighbor interaction operator can be written in the form

$$\begin{aligned} \langle F_1^{bqcf,lin}, u \rangle &= \|u_x\|^2 \\ \langle F_2^{bqcf,lin}, u \rangle &= 4\|u_x\|^2 + a^2 16A \left\| \sqrt{\beta} u_{xx} \right\|^2 + R + S. \end{aligned} \quad (7.4)$$

where R and S are given by:

$$R = -a^2 A \int \beta_{xx} (u_x)^2 dx, \quad S = a^2 A \int \beta_{xx} (u_{xx} u) dx. \quad (7.5)$$

Proof. Since the proof of the first identity of Lemma 7.1 is straightforward and utilizes the same properties, the proof for the second-neighbor interaction operator will be given. The main tool used is integration by parts based on the periodic boundary conditions.

$$\begin{aligned} \langle F_2^{bqcf}, u, u \rangle &= \int (\beta a^2 B u_{xxxx} - u_{xx}) u dx \\ &= \int -u_{xx} u dx + \int \beta a^2 A u_{xxxx} u dx \\ &= \int (u_x)^2 dx + a^2 A \int \beta u u_{xxxx} dx \\ &= \|u_x\|^2 - a^2 A \int (\beta u)_x u_{xxx} dx \\ &= \|u_x\|^2 + a^2 A \left\| \sqrt{\beta} u_{xx} \right\|^2 + a^2 A \int \beta_x (u_x)_x^2 dx - a^2 A \int \beta_x (u u_{xx})_x dx \\ &= \|u_x\|^2 + a^2 A \left\| \sqrt{\beta} u_{xx} \right\|^2 - a^2 A \int \beta_{xx} (u_x)^2 dx + a^2 A \int \beta_{xx} (u_{xx} u) dx \\ &= \|u_x\|^2 + a^2 A \left\| \sqrt{\beta} u_{xx} \right\|^2 + R + S. \end{aligned} \quad (7.6)$$

Using the continuous analysis as a road-map, we thus derive the discrete analysis in Section 3. \square

7.3 Symbols and Notation

superscript e.g., ' , ''	first order backward finite difference, second order central finite difference, etc. for the discrete case
subscript e.g., x, xx	first derivative, second derivative, etc. for the continuous case
$\frac{\delta}{\delta u_\ell}$	first order variation evaluated at u_ℓ
$\frac{d}{dx}$	derivative evaluated at x
$\ \cdot\ _{\ell_2}$	ℓ_2 -norm
$\ \cdot\ _{\ell_\infty}$	∞ -norm
$\ \cdot\ _{\ell_2(\Omega^b)}$	2-norm evaluated on the blending region Ω_b
$ \cdot _{H^1}$	discrete H^1 semi-norm
$\langle \cdot, \cdot \rangle$	inner product
ϕ	atomistic interaction potential per unit cell
$(\cdot)^c$	continuum equation
$(\cdot)^a$	atomistic equation
$(\cdot)^{lin}$	linearized equation
$(\cdot)^{bqcf}$	force-based blended equation
Ω	whole domain
Ω^a	atomistic domain
Ω^c	continuum domain
Ω^b	blending domain
β	blending function
L	number of atoms within the blending region Ω_b
a	lattice spacing constant
y_ℓ	deformation at ℓ
u_ℓ	displacement at ℓ
E	energy equation
$F_{\ell,k}$	force equation at atom ℓ with k^{th} neighbor interaction
F_ℓ	force equation at atom ℓ with the summation of all neighbor interaction
F_k	force equation with k^{th} neighbor interaction with the summation of all atoms
α	parameter in the Morse Potential
N	number of neighbors within the interaction range
M	half number of atoms in the atomistic chain
F^{ext}	external force

References

- [1] M. D'Elia and M. Gunzburger. Optimal distributed control of nonlocal steady diffusion problems. *SIAM Journal on Control and Optimization*, 52:243–273, 2014.
- [2] Marta D'Elia, Xingjie Li, Pablo Seleson, Xiaochuan Tian, and Yue Yu. A review of local-to-nonlocal coupling methods in nonlocal diffusion and nonlocal mechanics. *To appear on Journal of Peridynamics and Nonlocal Modeling*, 2020.
- [3] Marta D'Elia, Mauro Perego, Pavel Bochev, and David Littlewood. A coupling strategy for nonlocal and local diffusion models with mixed volume constraints and boundary conditions. *Computers and Mathematics with applications*, 71(11):2218–2230, 2015.
- [4] Qiang Du, Max Gunzburger, R Lehoucq, and Kun Zhou. Analysis and approximation of nonlocal diffusion problems with volume constraints. *SIAM Review*, 56:676–696, 2012.
- [5] Qiang Du and Robert Lipton. Peridynamics, fracture, and nonlocal continuum models. *SIAM News*, 47(3), 2014.
- [6] Weinan E. *Principles of multiscale modeling*. Cambridge University Press, 2011.

- [7] Ivan G. Graham, Thomas Y. Hou, Omar Lakkis, and Robert Scheichl. *Numerical analysis of multiscale problems*. Springer, 2012.
- [8] Ivan Kondov and Godehard Sutmann. *Multiscale modeling methods for applications in materials science*. Forschungszentrum Julich, 2013.
- [9] X. Li, M. Luskin, and C. Ortner. Positive definiteness of the blended force-based quasicontinuum method. *Multiscale Modeling & Simulation*, 10(3):1023–1045, 2012.
- [10] M. Luskin and C. Ortner. Atomistic-to-continuum-coupling. *Acta Numerica*, 22(4):397–508, 2013.
- [11] R. Miller and E. Tadmor. A unified framework and performance benchmark of fourteen multiscale atomistic/continuum coupling methods. *Modelling and Simulation in Materials Science and Engineering*, 17(5):053001, 2009.
- [12] R. Phillips. *Crystals, defects and microstructures: modeling across scales*. Cambridge University Press, 2001.
- [13] Pablo Seleson, Samir Beneddine, and Serge Prudhomme. A force based coupling scheme for peridynamics and classical elasticity. *Computational Materials Science*, 66:34–49, 2013.
- [14] Pablo Seleson, Youn Doh Ha, and Samir Beneddine. Concurrent coupling of bond-based peridynamics and the Navier equation of classical elasticity by blending. *Journal for Multiscale Computational Engineering*, 13:91–113, 2015.
- [15] A. V. Shapeev. Consistent energy-based atomistic/continuum coupling for two-body potentials in one and two dimensions. *SIAM J. Multiscale Model. Simul.*, 9(3):905–932, 2011.
- [16] Stewart Silling. Reformulation of elasticity theory for discontinuities and long-range forces. *Journal of the Mechanics and Physics of Solids*, 48:175–209, 2000.
- [17] E. Tadmor and R. Miller. *Modeling materials continuum, atomistic and multiscale techniques*. Cambridge University Press, first edition, 2011.
- [18] N. Trask, H. You, Y. Yu, and M. L. Parks. An asymptotically compatible meshfree quadrature rule for nonlocal problems with applications to peridynamics. *Computer Methods in Applied Mechanics and Engineering*, 343:151–165, 2019.
- [19] Kerstin Weinberg and Anna Pandolfi. *Innovative numerical approaches for multi-field and multi-scale problems: in honor of Michael Ortiz’s 60th birthday*. Springer, 2016.
- [20] H. You, Y. Yu, and D. Kamensky. An asymptotically compatible formulation for local-to-nonlocal coupling problems without overlapping regions. *Computer Methods in Applied Mechanics and Engineering*, 366, 2020.